Photoelectron momentum distributions of molecules in bichromatic circularly polarized attosecond UV laser fields

Kai-Jun Yuan,* Szczepan Chelkowski, and André D. Bandrauk†
Laboratoire de Chimie Théorique, Faculté des Sciences, Université de Sherbrooke, Sherbrooke, Québec J1K 2R1, Canada
(Received 14 March 2016; published 27 May 2016)

We theoretically investigate molecular photoelectron momentum distributions (MPMDs) by bichromatic [frequencies (ω_1,ω_2)] circularly polarized attosecond UV laser pulses. Simulations performed on aligned single-electron H_2^+ by numerically solving the corresponding three-dimensional time-dependent Schrödinger equation within a static nucleus frame show that MPMDs exhibit a spiral structure for both *co-rotating* and *counter-rotating* schemes. Results are analyzed by attosecond perturbation ionization models. Coherent electron wave packets created, respectively, by the two color pulses in the continuum interfere with each other. Photoionization distributions are functions of the photoelectron momentum p and the ejection angle θ, thus leading to *spiral* MPMDs. The dependence of spiral MPMDs on the time delay between the bicircular pulses and their relative phases is also presented. The spiral interference patterns are determined by the helicities and frequencies (ω_1,ω_2) of the bicircular fields. It is also found that the spiral patterns are sensitive to the molecular alignment and suppressed by two-center ionization interference, thus offering new tools for imaging molecular geometry.

DOI: 10.1103/PhysRevA.93.053425

I. INTRODUCTION

Imaging and control of molecular reaction dynamics are achieved in the laboratory nowadays with ultrashort ultrafast laser pulses in the femtosecond (1 fs $= 10^{-15}$ s) time regime associated with nuclear motion [1,2]. The recent advent of ever shorter laser pulses from high-order harmonic generation (HHG) [3,4] has opened an analogous field of research, i.e., investigating electron dynamics at its natural attosecond (1 as $= 10^{-18}$ s) time scale and subnanometer dimension, in which the nuclei are essentially frozen [5–8]. To date the shortest single pulse, of 67-as duration, has been achieved with HHG by linearly polarized IR pulses in atoms [9]. One can thus watch pure electronic quantum effects through attosecond imaging, leading to the creation of electron movies [10]. Recently, circularly polarized laser pulses have been shown to be important for investigating electron dynamics, such as recollision of electrons in double ionization [11,12] and generation of plasmas in air [13]. With the creation of "spinning" continuum electrons, time-dependent electronic ring currents can be induced in molecules, as new sources of intense internal magnetic fields [14,15], which are of growing interest in areas such as magneto-optical recording and superconductivity materials.

Bichromatic circularly polarized laser pulses are new tools for investigating electron dynamics in strong-field ionization of atoms, molecules, and even surfaces, following early experiments on polarization properties of high-intensity HHG [16]. It was shown first in 1995 that *co-rotating* or *counter-rotating* intense ultrafast circularly polarized pulses with the same or opposite helicities induce recollision of electrons with parent ions, thus ensuring efficient HHG [17,18], as opposed to single circular pulses, where recollision is suppressed as electrons with the maximum energy $2U_p$ "spin" out [19], where $U_p = I_0/4m_e\omega^2$ is the ponderomotive energy for intensity I_0 and angular frequency ω. Detailed study of the polarizations of the harmonics showed these to be circularly polarized, corresponding to angular momentum conservation rules, but with varying helicities [20–22]. Normally, due to the different helicities of the harmonics, circularly polarized attosecond pulses are not produced from superposition of such harmonics. Much effort has been devoted to circularly polarized attosecond pulse generation by HHG in bichromatic fields. A scheme based on nonzero angular momenta of electronic states has recently been proposed, with counter-rotating circularly polarized IR-visible laser pulses [23,24]. Alternatively, we have shown that combination of a circularly polarized IR laser and a linearly polarized, much lower (terahertz) laser with intense pulse intensities leads to single-trajectory recollision and circularly polarized HHG, from which one can generate single, circularly polarized attosecond pulses [25]. Counter-rotating circularly polarized laser pulses also lead to the technique of double-optical gating for producing isolated elliptically polarized attosecond pulses [26]. Such new ultrashort pulses are now being adopted to probe atomic and molecular structure by photoelectron momentum distributions [27] and electronic currents as sources of attosecond magnetic-field pulse generation [28]. In the latter induced electronic currents exhibit a sensitivity to the field helicity and phases. Two time-delayed, circularly polarized attosecond UV pulses of the same frequency produce spiral electron vortices in atomic photoionization momentum distributions [29]. It is found that the *vortex* patterns can only be observed for two oppositely handed, i.e., counter-rotating, circularly polarized fields and are absent for the same helicity (co-rotating pulses).

In the present work molecular photoionization by various frequency combinations of co-rotating and counter-rotating bichromatic circularly polarized attosecond UV pulses is presented from numerical solutions of the three-dimensional (3D) time-dependent Schrödinger equation (TDSE) of aligned

*kaijun.yuan@usherbrooke.ca
†andre.bandrauk@usherbrooke.ca

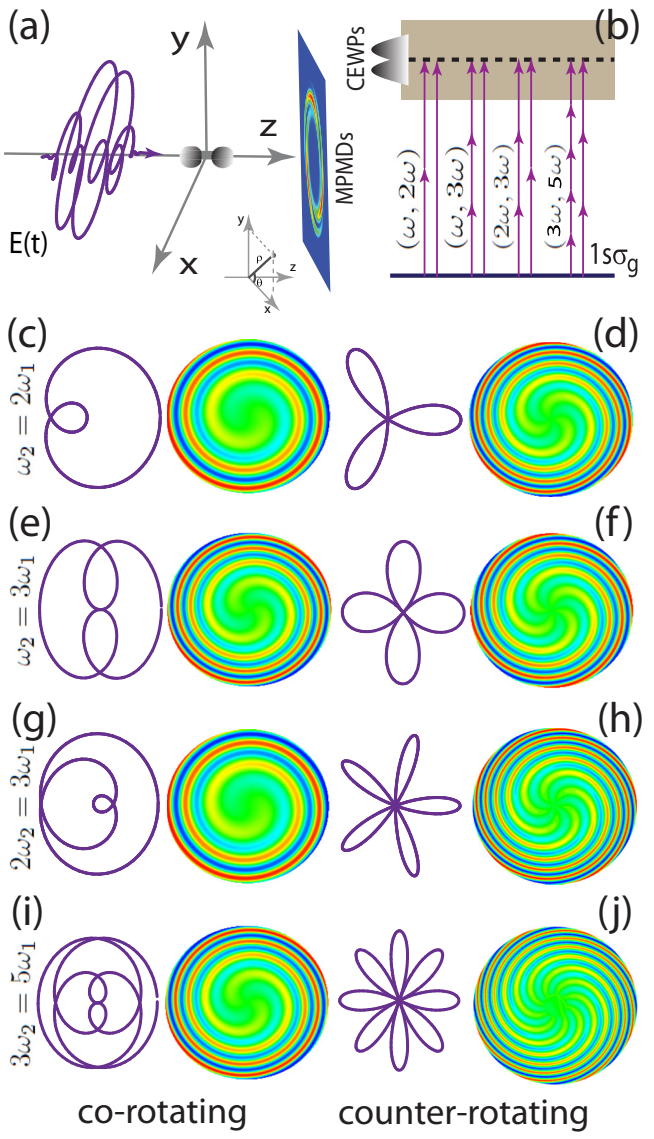

FIG. 1. (a) Illustrations of photoionization in the z-aligned molecular ion H_2^+ by bichromatic (ω_1,ω_2) circularly polarized attosecond UV laser pulses $\mathbf{E}(t)$. The ionizing laser pulse is polarized in the (x,y) or (ρ,θ) plane with $x=\rho\cos\theta$ and $y=\sin\theta$, propagating along the z axis parallel to the molecular axis. MPMDs are mainly localized in the perpendicular laser polarization (x,y) plane. (b) Multiple-pathway ionization interference by bichromatic (ω_1,ω_2) fields. The combined bichromatic circularly polarized laser electric fields $\mathbf{E}(t)$ and corresponding photoelectron spiral interference patterns obtained from attosecond perturbation ionization models at frequencies of (c, d) $\omega_2=2\omega_1$, (e, f) $\omega_2=3\omega_1$, (g, h) $2\omega_2=3\omega_1$, and (i, j) $3\omega_2=5\omega_1$, with (c), (e), (g), and (i) co-rotating and (d), (f), (h), and (j) counter-rotating components.

H_2^+ at equilibrium. We focus on the interference effects between coherent electron wave packets (CEWPs) created by, respectively, two-color circularly polarized UV pulses. We illustrate these pulse combinations in Fig. 1 for frequencies $\omega_2/\omega_1=2$, 3, 3/2, and 5/3. More general combinations have recently been presented in a review [30], where it is shown that such pulses can be obtained by modulating the envelope of a single circularly polarized pulse [17,18]. The $\omega_2/\omega_1=5/3$ case, corresponding to $\lambda_1=1300$ nm and $\lambda_2=800$ nm, has recently been studied [31]. We take the counter-rotating case in Figs. 1(d), 1(f), 1(h), and 1(j) as a reference, in the (x,y) polarization plane [Fig. 1(b)], for which the bicircular electric field reads

$$E(t)=E_0 f(t)\begin{pmatrix}\cos\omega_1 t+\cos\omega_2 t\\ \sin\omega_1 t-\sin\omega_2 t\end{pmatrix}, \tag{1}$$

where E_0 and $f(t)$ are the pulse-field amplitude and envelope, respectively. In most cases, as illustrated in Fig. 1, the beating between the two-color components induces a periodic vanishing (zero) of the electric field $E(t)$ which is associated with recollision and HHG. This becomes obvious in a rotating frame at frequency $\Delta\omega=(\omega_1-\omega_2)/2$, which maps the total field-molecular Hamiltonian as first demonstrated in [17,18] by

$$H(x,y,t)=H_0+\Delta\omega l_z+2xE_0 f(t)\cos\bar{\omega}t, \tag{2}$$

where $l_z=-i(x\frac{\partial}{\partial y}+y\frac{\partial}{\partial x})$ and $\bar{\omega}=(\omega_1+\omega_2)$ and H_0 is the field-free molecular Hamiltonian. Thus in the rotating frame, an electron is under the influence of a Coriolis force due to angular momentum, in addition to a linearly polarized time-dependent field which induces tunneling ionization and recollision. The maximum recollision energy varies from the classical single linear polarization energy of $3.17U_p$ [3,4] when $\omega_1=\omega_2$ but is always smaller for $\omega_1\neq\omega_2$ [23]. Of note is that the counter-rotating field combination has the number of spiral electron currents equal to the numbers of field maxima and loops.

Spiral distributions of electron wave packets on spatiotemporal scales due to the helicity of circularly polarized pulses have been reported in the IR-visible regime for producing circularly or elliptically polarized HHG and attosecond pulse generation [32]. We present spiral interference patterns in such photoelectron momentum distributions. Attosecond perturbation ionization models are adopted to describe these distributions. It is found that the distributions are functions of the photoelectron momenta p, electron ejection angles θ, and relative carrier envelope phases (CEPs) ϕ and the time delay $\Delta\tau$ between the two circularly polarized pulses. Compared to photoionization by two equal-frequency circularly polarized laser pulses [29], spiral interference patterns in MPMDs can always be obtained for bichromatic processes with both co-rotating and counter-rotating components. We also study the influence of pulse wavelengths and molecular alignment on the spiral interference patterns.

The paper is arranged as follows: In Sec. II, we briefly describe the computational methods for time-dependent quantum electron wave-packet calculations from the corresponding TDSEs. The numerical results of MPMDs for aligned H_2^+ by intense bichromatic circularly polarized attosecond UV laser pulses with both co-rotating and counter-rotating components are presented and discussed in Sec. III. Attosecond perturbation ionization models are used to analyze the spiral interference pattern in MPMDs, and the effects of pulse frequencies and molecular geometry are also investigated. Finally, we summarize our findings in Sec. IV. Throughout this paper, atomic units (a.u.) $e=\hbar=m_e=1$ are used unless otherwise stated.

II. COMPUTATIONAL METHODS

For an aligned diatomic molecular ion interacting with a laser pulse, as illustrated in Fig. 1(a), the corresponding TDSE with static nuclei in cylindrical coordinates can be written as

$$i\frac{\partial}{\partial t}\psi(\mathbf{r},t) = H(\mathbf{r},t)\psi(\mathbf{r},t), \tag{3}$$

where the field-molecule Hamiltonian is $H(\mathbf{r},t) = T(\mathbf{r}) + V(\mathbf{r}) + \mathbf{r}\cdot\mathbf{E}(t)$ and $\mathbf{r} = (\rho,\theta,z)$ with $(x = \rho\cos\theta,\ y = \rho\sin\theta)$. $V(\mathbf{r})$ is the molecular Coulomb potential. The molecular kinetic energy term (Laplacian) is

$$T(\rho,\theta,z) = -\frac{1}{2\rho}\frac{\partial}{\partial\rho}\left(\rho\frac{\partial}{\partial\rho}\right) - \frac{1}{2\rho^2}\frac{\partial^2}{\partial\theta^2} - \frac{1}{2}\frac{\partial^2}{\partial z^2}. \tag{4}$$

The field-molecule interaction is treated in the length gauge with circularly polarized laser fields

$$\mathbf{E}(t) = \mathbf{E}_1(t) + \mathbf{E}_2(t), \tag{5}$$

with

$$\mathbf{E}_1(t) = E_0 f(t)[\hat{e}_x\cos(\omega_1 t + \phi_1) + \hat{e}_y\sin(\omega_1 t + \phi_1)] \tag{6}$$

and

$$\begin{aligned}\mathbf{E}_2(t) = E_0 f(t-\Delta\tau)\{&\hat{e}_x\cos[\omega_2(t-\Delta\tau)+\phi_2)\\ &\pm\hat{e}_y\sin[\omega_2(t-\Delta\tau)+\phi_2])\},\end{aligned} \tag{7}$$

where ϕ_1 and ϕ_2 are pulse CEPs and the sign $\pm$ denotes the helicity of (left- or right-handed) circularly polarized laser pulses. $\Delta\tau$ presents the time delay between the two pulses, $\mathbf{E}_1(t)$ and $\mathbf{E}_2(t)$. A temporal slowly varying envelope $f(t) = \sin^2(\pi t/T)$ of duration $T = n\tau$, where one optical cycle (o.c.) $1\tau = 2\pi/\omega$, is adopted.

We solve numerically the 3D $H_2{}^+$ TDSE using a five-point finite-difference method and fast Fourier transform technique combined with high-order split-operator methods [33]. The time step is fixed at $\Delta t = 0.01$ a.u. (1 a.u. = 24 as) and the spatial discretization is $\Delta\rho = \Delta z = 0.25$ a.u. (1 a.u. = $1a_0$, Bohr radius) for radial grid sizes $0 \leqslant \rho \leqslant 128$ a.u. and $|z| \leqslant 64$ a.u. and angle grid size $\Delta\theta = 0.01$ radian. To prevent unphysical effects due to the reflection of the wave packet from the boundary, a "mask function" with the form $\cos^{1/8}[\pi(\rho-\rho_a)/2\rho_{abs}]$ [34] is used at $\rho_{abs} = \rho_{\max} - \rho_a = 24$ a.u. with $\rho_{\max} = 128$ a.u.

For an intense high-frequency laser pulse, a quite large grid range must be used to obtain via Fourier transform the high energy of the ejected electron in the ionization spectra. In the present work we use an efficient method by calculating a radial flux (electron current density) $\mathcal{J}(t)$ to describe the ionization spectra, where the high kinetic energy of ionized electron can be accurately calculated. The electron wave function $\psi(\rho,\theta,z,t)$ generates the radial flux $\mathcal{J}(t)$ at an asymptotic point $\rho_f = 100$ a.u. before the wave packet is absorbed. At such a large asymptotic point ρ_f, the angular flux distributions can be ignored, i.e., $1/\rho_f\partial/\partial\theta|_{\rho_f}\hat{e}_\theta \ll \partial/\partial\rho|_{\rho_f}\hat{e}_\rho$. As a result we only need to consider the radial part of the electronic flux along the radial direction, $\partial/\partial\rho|_{\rho_f}\hat{e}_\rho$. At the boundary, the effects of the field on the outgoing electron can be ignored due to the short pulse duration. The time-independent energy-resolved angular differential yield (photoelectron spectra) is obtained by a Fourier transform from the exact time-dependent functions $\psi(\rho,\theta,z,t)$ in Eq. (3):

$$\begin{aligned}\psi(\theta,z,E)|_{\rho_f} &= \int_{t_p}^{\infty}\psi(\theta,z,t)|_{\rho_f}e^{iEt}dt,\\ \psi'(\theta,z,E)\,|_{\rho_f} &= \int_{t_p}^{\infty}\frac{\partial\psi(\theta,z,t)}{\partial\rho}|_{\rho_f}e^{iEt}dt,\\ \mathcal{J}(\theta,E) &\sim \mathrm{Re}\left[\frac{1}{2i}\int\psi'^{*}(\theta,z,E)|_{\rho_f}\psi(\theta,z,E)|_{\rho_f}dz\right],\end{aligned} \tag{8}$$

where t_p is the time after the pulse switches off. $E = p^2/2$ (in a.u.) is the kinetic energy of an ionized electron with wave vector $k = p = 2\pi/\lambda_e$ (in a.u.), and $p = (p_x^2 + p_y^2)^{1/2}$ is the momentum of a photoelectron of wavelength λ_e. Since only the radial electron flux is taken into account, we also define θ as the angle between the electron momentum $\mathbf{p}$ and the x polarization axis. With the transformation $p_x = p\cos\theta$ and $p_y = p\sin\theta$, we then obtain the 2D momentum distributions of photoelectrons from Eq. (8).

III. NUMERICAL RESULTS AND DISCUSSION

In this work we present two-color, circularly polarized, attosecond UV photoionization of the molecular ion $H_2{}^+$ at equilibrium $R_e = 2$ a.u., which has been used as a benchmark system for the essential concepts to understand ultrafast molecular reaction dynamics with intense laser pulses, e.g., [35,36]. The initial electron wave function $\psi(\mathbf{r},t=0)$ is prepared in the ground $1s\sigma_g$ state calculated by propagating an initial appropriate wave function in imaginary time using the zero-field TDSE in Eq. (3). The Keldysh parameter $\gamma = \sqrt{I_p/2U_p} > 1$, where I_p is the ionization potential, implies multiphoton ionization processes. Thus the modification of the ionization potential by the laser-induced Stark shift can be ignored. We consider two cases with molecular z and x alignments, i.e., the molecular R axis is parallel or perpendicular to the propagation direction of the circularly (x,y) polarized light [Fig. 1(a)]. Current laser alignment technology [37] allows for prealignments of molecular ions before ionization.

A. Photoionization by bichromatic co-rotating, $\omega_1 = 2\omega_2$, circularly polarized laser pulses

We first consider a photoionization process of z-aligned $H_2{}^+$ [Fig. 1(a)] by bichromatic circularly polarized attosecond UV laser pulses with co-rotating components, i.e., the same left-handed helicities in the (x,y) plane (Fig. 1). The pulse wavelengths are, respectively, $\lambda_1 = 60$ nm (angular frequency $\omega_1 = 0.76$ a.u.) and $\lambda_2 = 30$ nm ($\omega_2 = 1.52$ a.u.). We always fix the pulse durations at $T = 12\tau$, i.e., 6 cycles for $\lambda_1 = 60$ nm ($\tau_1 = 2\pi/\omega_1 = 2\tau$) and 12 cycles for $\lambda_2 = 30$ nm ($\tau_2 = 2\pi/\omega_2 = \tau$), corresponding to an FWHM (full width at half-maximum) of 596. We define one cycle duration of 30-nm pulses as the unit of $\tau = 4.13$ a.u. = 99.2 as. Since $I_p = 1.1$ a.u. corresponds to a laser wavelength $\lambda = 40$ nm, direct ionization is induced at λ_2, whereas two-photon ionization occurs at λ_1.

Figure 2 displays results of molecular photoionization by bichromatic co-rotating circularly polarized attosecond UV laser pulses at different time delays $\Delta\tau$ and relative CEPs ϕ.

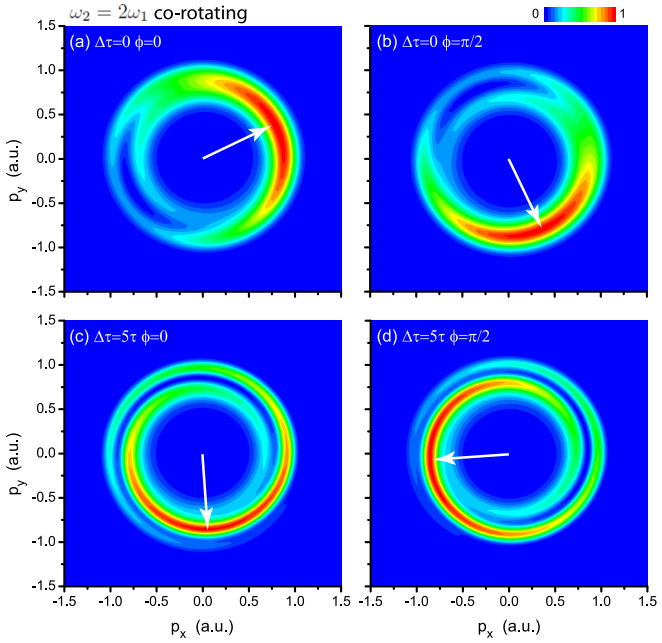

FIG. 2. MPMDs of z-aligned H_2^+ [Fig. 1(a)] in bichromatic perpendicular (x,y) circularly polarized attosecond UV laser pulses with *co-rotating* components, i.e., two left-handed pulses at wavelengths $\lambda_1 = 60$ nm ($\omega_1 = 0.76$ a.u.) and $\lambda_2 = 30$ nm ($\omega_2 = 1.52$ a.u.), intensity $I_0 = 5 \times 10^{14}$ W/cm^2 ($E_0 = 0.12$ a.u.), and FWHM = 596 as. (a) Pulse CEPs $\phi_1 = \phi_2 = 0$ ($\phi = 0$) and time delay $\Delta\tau = 0$; (b) $\phi_1 = 0$, $\phi_2 = \pi/2$ ($\phi = \pi/2$) and $\Delta\tau = 0$; (c) $\phi_1 = \phi_2 = 0$ ($\phi = 0$) and $\Delta\tau = 5\tau$ (496 as); and (d) $\phi_1 = 0$, $\phi_2 = \pi/2$ ($\phi = \pi/2$) and $\Delta\tau = 5\tau$.

One sees that MPMDs are sensitive to both the pulse CEP ϕ and the time delay $\Delta\tau$. At a time delay $\Delta\tau = 5\tau$ (496 as) MPMDs exhibit one diffuse momentum spiral structure in the polarization (p_x, p_y) plane, as shown in Figs. 2(c) and 2(d), whereas at zero time delay narrower rings are obtained, implying orientation [Figs. 2(a) and 2(b)] with asymmetry in the left-right polarization plane. Such bichromatic laser pulses can produce photoelectron wave packets with the same kinetic energies by combination of multiple multiphoton transitions and steer them through different pathways in the continuum, thus creating the interference effects of CEWPs in the photoelectron energy spectra. It is also found that varying the relative CEPs from $\phi = 0$ ($\phi_1 = \phi_2 = 0$) to $\pi/2$ ($\phi_1 = 0$ and $\phi_2 = \pi/2$) leads to clockwise rotations of MPMDs with a $\Delta\theta = 90^\circ$ angle in both time delays, $\Delta\tau = 0$ and $\Delta\tau = 5\tau$. Clearly, increasing time delays results in larger spirals and further rotations, thus suggesting a control tool for spirality and rotation.

It should be noted that for the cases with two identical-frequency, circularly polarized attosecond UV pulses as reported recently by Starace and coworkers [29], circularly symmetric patterns independent of the electron ejection angle are produced in photoelectron momentum distributions in atomic He. The corresponding momentum rings are also insensitive to the pulse CEPs. Electronic vortices are obtained by opposite helicity, i.e., counter-rotating, circularly polarized attosecond UV laser pulses [29]. By bichromatic circularly polarized UV laser pulses with co-rotating components, CEWPs with different angular momenta are created in the continuum after absorptions of one and two photons. Their interference effects result in angle-dependent distributions, i.e., an asymmetry in MPMDs. In the case of ionization by linearly polarized pulses, the asymmetry is also sensitive to the pulse CEPs [38]. However, for the processes by circularly polarized pulses, varying CEPs result in rotations of MPMDs. CEWPs are also functions of the photoelectron kinetic energies, thus leading to spiral photoelectron momentum distributions. We next use attosecond perturbation photoionization models [39,40] to describe the spiral interference structure of MPMDs in Fig. 2.

The spiral structure of MPMDs in Fig. 2 indicates the essential role of interference effects of CEWPs. For a combination of bichromatic circularly polarized laser pulses of frequencies ω_1 and $\omega_2 = 2\omega_1$, the electron can be ionized via multiple pathways to reach the same final energies in the continuum simultaneously, as illustrated in Fig. 1(b). For direct one-ω_2-photon ionization processes by laser pulses, the transition matrix element $\mathcal{W}^{(1)}$ can be expressed simply in the dipole form,

$$\mathcal{W}^{(1)} = \langle\psi_c|\mathbf{D}\cdot\mathbf{E}_2(\omega)|\psi_0\rangle e^{-i\eta_2} = \sigma^{(1)} f^{(1)}, \tag{9}$$

with the first-order ionization amplitude

$$\sigma^{(1)} = \langle\psi_c|DE_2(\omega)|\psi_0\rangle. \tag{10}$$

$\mathbf{E}_2(\omega) = \mathbf{e}E_2(\omega)$ is the pulse frequency shape as a Fourier transform of the ionizing pulse $\mathbf{E}_2(t)$. The scalar product

$$f^{(1)} = (\mathbf{n}\cdot\mathbf{e}_2)e^{-i\eta_2}, \tag{11}$$

where $|\psi_0\rangle$ and $|\psi_c\rangle$ are, respectively, the initial ground state and the continuum state. $\mathbf{D} = \mathbf{n}D$ is the electric dipole operator, $\mathbf{n}$ is its unit vector direction, and η_2 is the total phase of the pulse $\mathbf{E}_2$.

For photoionization with a circularly polarized laser pulse, the scalar product $(\mathbf{n}\cdot\mathbf{e})$ can be simply written as [39,40]

$$\mathbf{n}\cdot\mathbf{e} = \cos\theta + i\sin\theta, \tag{12}$$

where θ is the angle of the transition dipole moment between the x axis, i.e., the ejection angle of the photoelectron we define here. Then the final MPMDs for the ω_2 pulses have the simple form

$$\frac{dP^{(1)}_{\rm ion}}{dpd\Omega} = |\mathcal{W}^{(1)}|^2 = \alpha^{(1)}(p), \tag{13}$$

where $\alpha^{(1)}$ depends on the ionizing laser pulse and the initial electronic state, i.e., $|\sigma^{(1)}|^2$, and the photoionization distributions show a ring structure with momentum radii $p = \sqrt{2(\omega_2 - I_p)}$ for an ionization potential I_p.

For the two-$(\omega_1 + \omega_1)$-photon nonresonant ionization, the transition matrix element can be expressed as [41]

$$\mathcal{W}^{(2)} = \sigma^{(2)} f^{(2)}, \tag{14}$$

with the ionization amplitude

$$\sigma^{(2)} \sim \sum_n \frac{\langle\psi_c|DE_1(\omega)|\psi_n\rangle\langle\psi_n|DE_1(\omega)|\psi_0\rangle}{E_{1s\sigma_g} - E_{ni} + \omega_1 + i\Gamma}, \tag{15}$$

where ψ_n and E_{ni} are the wave function and energy of the intermediate (virtual) electronic state and Γ is the level width.

The scalar product

$$f^{(2)} = (\mathbf{n}\cdot\mathbf{e}_1)^2 e^{-2i\eta_1}, \tag{16}$$

where η_1 is the total pulse phase of $\mathbf{E}_1$, describes the corresponding angular distributions. The corresponding distributions are also independent of the photoelectron ejection angle; i.e., one obtains a ring structure,

$$\frac{dP_{\rm ion}^{(2)}}{dpd\Omega} = |\mathcal{W}^{(2)}|^2 = \alpha^{(2)}(p), \tag{17}$$

where the coefficient $\alpha^{(2)}(p) \sim |\sigma^{(2)}|^2$.

For photoionization by bichromatic co-rotating ($\mathbf{e}_1 = \mathbf{e}_2$) circularly polarized laser pulses, that is, simultaneous two-($\omega_1+\omega_1$)-photon amplitudes in Eq. (14) and one-($\omega_2 = 2\omega_1$)-photon ionization amplitude in Eq. (9), the total transition probability is the square of the two amplitudes, with an interference term of the cross products of the two one-photon and one two-photon ionization amplitudes, namely,

$$\frac{dP_{\rm ion}^{+}}{dpd\Omega} = \frac{dP_{\rm ion}^{(1)}}{dpd\Omega} + \frac{dP_{\rm ion}^{(2)}}{dpd\Omega} + \frac{dP_{\rm ion}^{(1,2),+}}{dpd\Omega}, \tag{18}$$

where $dP_{\rm ion}^{(1,2),+}/dpd\Omega$ is the interference term, which can be simply written as [42,43]

$$\begin{aligned}\frac{dP_{\rm ion}^{(1,2),+}}{dpd\Omega} &= \mathcal{W}^{(1)*}\mathcal{W}^{(2)} + \mathcal{W}^{(1)}\mathcal{W}^{(2)*} \\ &= \alpha^{(1,2)}(p) f^{(1,2)},\end{aligned} \tag{19}$$

where $\mathcal{W}^{(1)}$ and $\mathcal{W}^{(2)}$ are, respectively, the transition matrix elements of the one- and two-photon absorption amplitudes in Eqs. (9) and (14), and $\alpha^{(1,2)}(p)$ is their corresponding interference amplitude. The angular scalar product $f^{(1,2)}$ can be expressed as [42]

$$f^{(1,2)} = f^{(1)*} f^{(2)} + f^{(1)} f^{(2)*} = 2\cos(\theta + \Delta\eta). \tag{20}$$

The total phase difference $\Delta\eta$ between the transition amplitudes for the two-pathway ionizations is the sum of difference phases of the laser pulses $\Delta\phi$ and $\Delta\xi$, that is, $\Delta\eta = \Delta\phi + \Delta\xi$ with $\Delta\phi = 2\phi_1 - \phi_2$ and $\Delta\xi = (p^2/2 - E_{1s\sigma_g})\Delta\tau$. Then the total angular distributions can finally be written as sums of direct and interfering photoionization distributions:

$$\frac{dP_{\rm ion}^{+}}{dpd\Omega} = \alpha^{(1)}(p) + \alpha^{(2)}(p) + 2\alpha^{(1,2)}(p)\cos(\theta + \Delta\eta). \tag{21}$$

The interference coefficient $\alpha^{(1,2)}(p)$ is determined by the intensities of the bichromatic laser pulses.

From Eq. (21) we see that MPMDs are composed of two angle-independent ionization components, $\alpha^{(1)}(p)$ and $\alpha^{(2)}(p)$, and their interference. The two direct ionization distributions are mainly proportional to the photoelectron momentum p with a ring structure. The interference term is a function of the momentum p and ejection angle θ of the photoelectron and phase difference $\Delta\eta = \Delta\phi + \Delta\xi$, i.e., ϕ and $\Delta\tau$. Therefore altering the laser parameters varies the MPMDs. For the case at CEPs $\phi_1 = \phi_2 = 0$ and time delay $\Delta\tau = 0$, the distributions is simply expressed as $dP_{\rm ion}^{(1,2),+}/dpd\Omega \sim \alpha^{(1,2)}(p)\cos\theta$. Asymmetric distributions thus are obtained with respect to the perpendicular y axis along $\theta = 0^\circ$ and 180°, as shown in Fig. 2(a). The distributions are mainly localized in the right half-plane since $\cos 0 = 1$. Due to the helicity of the pulse, a 35° rotation angle of MPMDs is induced with respect to the polarization and molecular internuclear axes [44]. Therefore the maximum and minimum values of MPMDs occur, respectively, at $\theta = 35^\circ$ and 215°. For photoionization at the CEP $\phi = \phi_2 = \pi/2$, the interference angular term $f^{(1,2)}$ shifts $\Delta\eta = \Delta\phi = \pi/2$. As a result, the MPMDs rotate clockwise with an angle of $\Delta\theta = 90^\circ$, i.e., $\cos(\theta + \pi/2)$, as shown in Fig. 2(b).

For the photoionization case at a time delay $\Delta\tau = 5\tau = 496$ as in Figs. 2(c) and 2(d), MPMDs exhibit the signature of a spiral structure. As shown in Eqs. (19) and (20), the interference distributions can be simply written as $dP_{\rm ion}^{(1,2),+}/dpd\Omega \sim \alpha^{(1,2)}(p)\cos[\theta + \Delta\phi + (p^2/2 - E_{1s\sigma_g})\Delta\tau]$, where $2\omega_1 = \omega_2 = p^2/2 - E_{1s\sigma_g}$, as illustrated in Fig. 1(c). Therefore, the minima and maxima of distributions occur, respectively, at

$$\theta = (2n+1)\pi - [\Delta\phi + (p^2/2 - E_{1s\sigma_g})\Delta\tau], \tag{22}$$

and

$$\theta = 2n\pi - [\Delta\phi + (p^2/2 - E_{1s\sigma_g})\Delta\tau], \tag{23}$$

where $n = 0, \pm1, \pm2, \ldots$). For the case at the angles

$$\theta = (2n+1/2)\pi - [\Delta\phi + (p^2/2 - E_{1s\sigma_g})\Delta\tau], \tag{24}$$

$dP_{\rm ion}^{(1,2),+}/dpd\Omega = 0$, no interference occurs. Equations (22)–(24) show that the ejection angle θ depends on the product of the photoelectron momentum p and the time delay $\Delta\tau$, thus giving rise to the spiral structure of MPMDs.

For two identical circularly polarized pulses at $\omega_1 = \omega_2$, the angular scale $f^{(1,2)}$ in Eq. (20) is

$$f^{(1,2)} = 2\cos(\Delta\eta), \tag{25}$$

independent of the photoelectron ejection angle θ. As a result, electron momentum rings are observed [29]. For co-rotating photoionization processes, the frequency difference ($\omega_1 \neq \omega_2$) results in angle dependence of MPMDs, thus giving rise to interference spiral patterns.

B. MPMDs for counter-rotating $\omega_2 = 2\omega_1$ schemes

In Fig. 3 we show photoionization of H_2^+ for a counter-rotating scheme with bichromatic, circularly polarized attosecond UV laser pulses with opposite helicities, i.e., a left-handed $\lambda_1 = 60$ nm pulse and a right-handed $\lambda_2 = 30$ nm pulse. The molecule is also prealigned along the z axis, i.e., the molecular R axis is perpendicular to the polarization (x,y) plane. The other laser parameters are the same as those used for the co-rotating scheme in Fig. 2. MPMDs at two pulse CEPs, $\phi = 0$ [Figs. 3(a) and 3(c)] and $\phi = \pi/2$ [Figs. 3(b) and 3(d)], and two time delays, $\Delta\tau = 0$ [Figs. 3(a) and 3(b)] and $\Delta\tau = 5\tau = 496$ as [Figs. 3(c) and 3(d)], are presented, respectively.

In Fig. 3 one sees that for the counter-rotating scheme MPMDs in the polarization (x,y) plane exhibit the signature of a spiral structure again, which is sensitive to the time delay $\Delta\tau$ and CEPs ϕ_1 and ϕ_2 of the bichromatic fields. At a time delay $\Delta\tau = 5\tau = 496$ as, in Figs. 3(c) and 3(d), spiral MPMDs are obtained, whereas at $\Delta\tau = 0$ three angle nodes are produced in MPMDs, with an interval of 120°. The

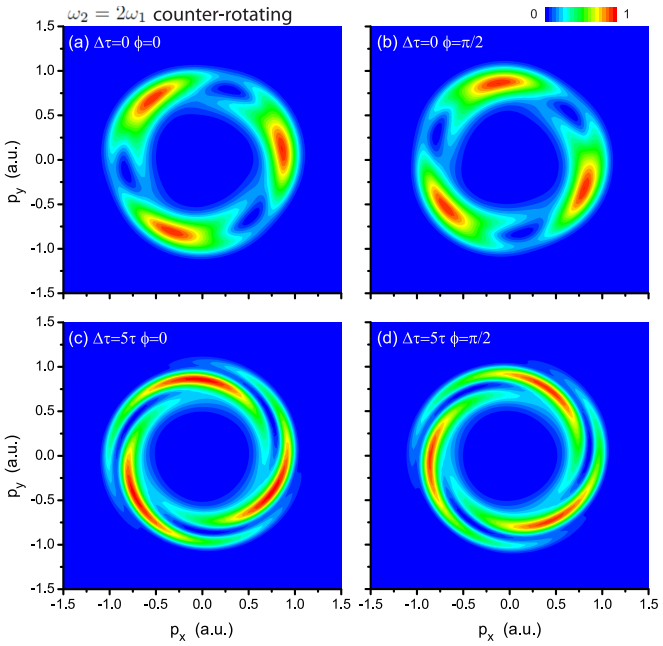

FIG. 3. MPMDs of z-aligned H_2^+ [Fig. 1(a)] in bichromatic perpendicular (x,y) circularly polarized attosecond UV laser pulses with *counter-rotating* components, i.e., one left-handed $\lambda_1 = 60$ nm ($\omega_1 = 0.76$ a.u.) and one right-handed $\lambda_2 = 30$ nm ($\omega_2 = 1.52$ a.u.) pulse at intensity $I_0 = 5 \times 10^{14}$ W/cm^2 ($E_0 = 0.12$ a.u.) and FWHM = 596 as. (a) Pulse CEPs $\phi_1 = \phi_2 = 0$ ($\phi = 0$) and time delay $\Delta\tau = 0$; (b) $\phi_1 = 0$, $\phi_2 = \pi/2$ ($\phi = \pi/2$) and $\Delta\tau = 0$; (c) $\phi_1 = \phi_2 = 0$ ($\phi = 0$) and $\Delta\tau = 5\tau$ (496 as); and (d) $\phi_1 = 0$, $\phi_2 = \pi/2$ ($\phi = \pi/2$) and $\Delta\tau = 5\tau$ (496 as).

spiral MPMDs arise from the interference effects of CEWPs by the two-color circularly polarized pulses, similar to Fig. 2. As the pulse CEPs change from $\phi_1 = \phi_2 = 0$ to $\phi_1 = 0$ and $\phi_2 = \pi/2$ ($\phi = \phi_2 - \phi_1 = \pi/2$), MPMDs rotate clockwise at an angle of $\Delta\theta = 30^\circ$. Compared to the co-rotating processes in Fig. 2, more angle nodes and spiral bursts are produced in the counter-rotating cases. The difference reflects the helicity effects of the combined fields on the photoionization.

We also use the attosecond perturbation ionization model to understand the spiral interference patterns in Fig. 3. As shown in Eq. (18) the total distributions of photoionization are sums of the two-photon ω_1 and one-photon ω_2 processes and their interference. The distributions $dP_{\rm ion}^{(1)}/dpd\Omega = |\mathcal{W}^{(1)}|^2$ and $dP_{\rm ion}^{(2)}/dpd\Omega = |\mathcal{W}^{(2)}|^2$ are the same as the co-rotating photoionization processes, which are a function of the photoelectron momentum p and insensitive to the helicities of the circularly polarized UV laser pulses. For the counter-rotating case with $\mathbf{e}_1 = \mathbf{e}_2^*$, the interference term reads

$$\frac{dP_{\rm ion}^{(1,2),-}}{dpd\Omega} = \mathcal{W}^{(1)*}\mathcal{W}^{(2)} + \mathcal{W}^{(1)}\mathcal{W}^{(2)*} = 2\alpha^{(1,2)}(p)\cos(3\theta + \Delta\eta), \quad (26)$$

where $\alpha^{(1,2)}(p)$ is the interference amplitude and the angular scale $f^{(1,-2)} = \cos(3\theta + \Delta\eta)$ depends on the ejection angle θ and the pulse phase difference $\Delta\eta = \Delta\phi + \Delta\xi$ with $\Delta\phi = 2\phi_1 + \phi_2$.

From Eq. (26) one sees that the interference term is a function of the photoelectron momenta p, ejection angles θ, pulse CEPs ϕ ($\Delta\phi$), and time delay $\Delta\tau$ ($\Delta\xi$). Therefore under particular conditions, spiral interference patterns can be observed in MPMDs, as analyzed above for the co-rotating process. For the interference distributions in Eq. (26), the extreme interferences occur at, respectively,

$$\theta = 2n\pi/3 - [\Delta\phi + (p^2/2 - E_{1s\sigma_g})\Delta\tau]/3 \quad (27)$$

for the maxima,

$$\theta = (2n+1)\pi/3 - [\Delta\phi + (p^2/2 - E_{1s\sigma_g})\Delta\tau]/3 \quad (28)$$

for the minima, and

$$\theta = (n+1/2)\pi/3 - [\Delta\phi + (p^2/2 - E_{1s\sigma_g})\Delta\tau]/3 \quad (29)$$

for the zero values of $dP_{\rm ion}^{(1,2),-}/dpd\Omega$. One sees that the maxima and minima are replicated with a period of $2\pi/3$, thus the photoionization distributions exhibit three bursts of spiral patterns, and the corresponding angle shift $\Delta\theta = \Delta\phi/3 = \pi/6$, i.e., 30°. For the case of two oppositely circularly polarized pulses at the same frequencies $\omega_1 = \omega_2$, the corresponding angular factor $f^{(1,-1)}$ can be expressed as

$$f^{(1,-1)} = 2\cos(2\theta + \Delta\eta), \quad (30)$$

with $\Delta\phi = \phi_1 + \phi_2$. Obviously, spiral interference patterns can be obtained in MPMDs [29].

C. Effects of pulse frequencies on interference spiral patterns

We next study the effect of varying the pulse frequencies ω_1 and ω_2 on the spiral interference patterns in MPMDs by bichromatic circularly polarized attosecond UV laser pulses in Fig. 1(b). The photoionization processes at frequencies $m_1\omega_1 = m_2\omega_2$ are taken into account where interference of photoelectron occurs at the same kinetic energies. At frequencies $\omega_2 = 3\omega_1$, the interference photoionization distributions can be expressed as, perturbatively,

$$\frac{dP_{\rm ion}^{(1,3),+}}{dpd\Omega} = 2\alpha^{(1,3)}(p)\cos(2\theta + \Delta\eta), \quad (31)$$

with co-rotating components, and

$$\frac{dP_{\rm ion}^{(1,3),-}}{dpd\Omega} = 2\alpha^{(1,3)}(p)\cos(4\theta + \Delta\eta), \quad (32)$$

with counter-rotating components, where the total phase difference is $\Delta\eta = \Delta\phi + \Delta\xi$. The pulse CEP difference reads $\Delta\phi = 3\phi_1 - \phi_2$ for co-rotating cases and $\Delta\phi = 3\phi_1 + \phi_2$ for counter-rotating schemes. The combined laser fields and corresponding interference patterns are also illustrated in Figs. 1(e) and 1(f). One sees that the spiral structure can be produced as well in the polarization plane under particular conditions of $\Delta\eta$, i.e., a time delay $\Delta\tau$. There are two spiral interference bursts in MPMDs for the co-rotating case, whereas four pattern bursts appear in the counter-rotating scheme.

Similar results can be obtained for the bichromatic photoionization processes at frequencies $2\omega_2 = 3\omega_1$ and $3\omega_2 = 5\omega_1$. At $2\omega_2 = 3\omega_1$, an interference between three ($\omega_1 + \omega_1 + \omega_1$) and two-($\omega_2 + \omega_2$)-photon ionization processes occurs as well. The corresponding interference distributions for the

co-rotating case read

$$\frac{dP_{\rm ion}^{(2,3),+}}{dpd\Omega} = 2\alpha^{(2,3)}(p)\cos(\theta + \Delta\eta), \tag{33}$$

and those for the counter-rotating case,

$$\frac{dP_{\rm ion}^{(2,3),-}}{dpd\Omega} = 2\alpha^{(2,3)}(p)\cos(5\theta + \Delta\eta), \tag{34}$$

where the total phase difference $\Delta\eta = \Delta\phi + \Delta\xi$. We define the pulse CEP difference as $\Delta\phi = 3\phi_1 - 2\phi_2$ for co-rotating cases and $\Delta\phi = 3\phi_1 + 2\phi_2$ for counter-rotating schemes. At $3\omega_2 = 5\omega_1$ in Figs. 1(i) and 1(j), interference distributions for the co-rotating case are

$$\frac{dP_{\rm ion}^{(3,5),+}}{dpd\Omega} = 2\alpha^{(3,5)}(p)\cos(2\theta + \Delta\eta), \tag{35}$$

and those for the counter-rotating case,

$$\frac{dP_{\rm ion}^{(3,5),-}}{dpd\Omega} = 2\alpha^{(3,5)}(p)\cos(8\theta + \Delta\eta), \tag{36}$$

with the total phase difference $\Delta\eta = \Delta\phi + \Delta\xi$, where $\Delta\phi = 5\phi_1 - 3\phi_2$ for co-rotating cases and $\Delta\phi = 5\phi_1 + 3\phi_2$ for counter-rotating schemes. Spiral interference patterns can also be produced from Eqs. (33)–(36); see also Figs. 1(g)–1(j).

In Fig. 4 we display the simulated results of photoionization for z-aligned H_2^+ by bichromatic (ω_1,ω_2), circularly polarized attosecond UV pulses with co-rotating and counter-rotating components. Three cases are taken into account at frequencies $\omega_2 = 3\omega_1$, i.e., $\omega_1 = 0.506$ a.u. ($\lambda_1 = 90$ nm) and $\omega_2 = 1.52$ a.u. ($\lambda_2 = 30$ nm), in Figs. 4(a) and 4(b); $2\omega_2 = 3\omega_1$, i.e., $\omega_1 = 0.506$ a.u. ($\lambda_1 = 90$ nm) and $\omega_2 = 0.76$ a.u. ($\lambda_2 = 60$ nm), in Figs. 4(c) and 4(d); and $3\omega_2 = 5\omega_1$, i.e., $\omega_1 = 0.304$ a.u. ($\lambda_1 = 150$ nm) and $\omega_2 = 0.506$ a.u. ($\lambda_2 = 90$ nm), in Figs. 4(e) and 4(f). The time delay between the two pulses is $\Delta\tau = 4.5\tau = 446$ as. We always fix the pulse intensity and FWHM at $I_0 = 5 \times 10^{14}$ W/cm^2 ($E_0 = 0.12$ a.u.) and 596 as. Pulse CEPs are also set at $\phi_1 = \phi_2 = 0$. One sees that the numerical results in Fig. 4 are in good agreement with the predictions in Eqs. (31)–(36) [Figs. 1(e)–1(j)]. Clear interference spiral patterns are produced in MPMDs, similar to the $\omega_2 = 2\omega_1$ photoionization processes in Figs. 2 and 3. Altering the pulse frequencies ω_1 and ω_2 also varies the spiral bursts in MPMDs. For the photoionization at frequencies $\omega_2 = 3\omega_1 = 1.52$ a.u., there are two bursts for the co-rotating case in Fig. 4(a), whereas four bursts are induced for the counter-rotating scheme in Fig. 4(b). Upon decreasing the frequency ω_2 or increasing the wavelength λ_2 of the pulse $\mathbf{E}_2(t)$, i.e., $\omega_2 = 3\omega_1/2 = 0.76$ a.u. ($\lambda_2 = 60$ nm), only one spiral burst appears for the co-rotating ionization, similar to the $\omega_2 = 2\omega_1$ processes in Figs. 2(a) and 2(b). However, for the counter-rotating case, MPMDs exhibit five interference spiral bursts. Decreasing the pulse frequencies further at $3\omega_2 = 5\omega_1$, i.e., $\lambda_1 = 150$ nm and $\lambda_2 = 90$ nm, two and eight bursts of spiral interference patterns are obtained for the co-rotating and counter-rotating cases, respectively [Figs. 4(e) and 4(f)]. The dependence of the spiral bursts on the pulse frequencies ω_1 and ω_2 indicates the essential role of the combined vector fields in the multiple path ionization interference processes. Moreover, for the broad spectral bandwidth of attosecond pulses, the ionizations near the molecular threshold are also induced localized around the center of MPMDs in Fig. 4.

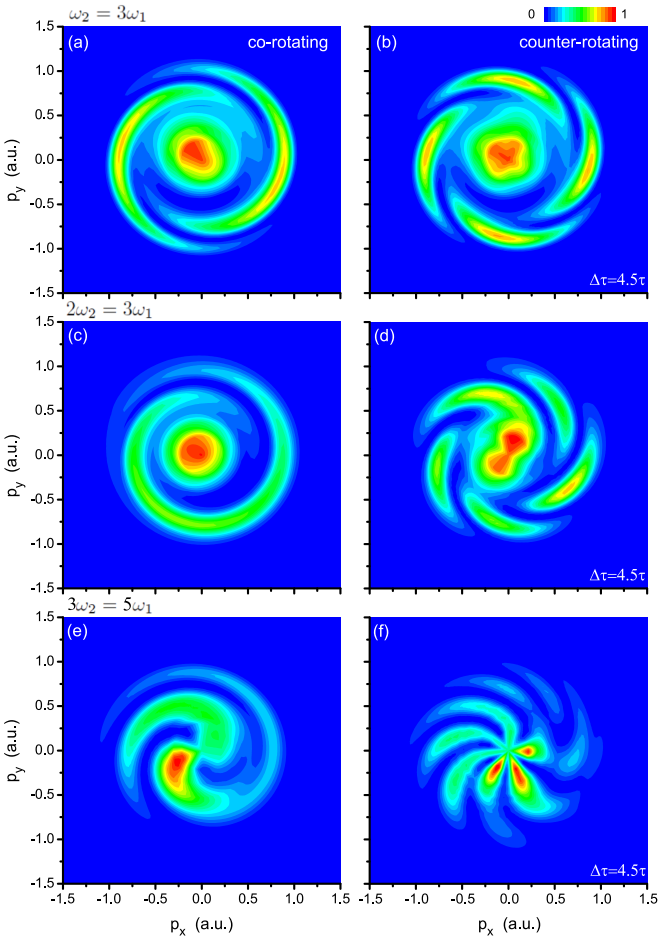

FIG. 4. MPMDs of z-aligned H_2^+ [Fig. 1(a)] in bichromatic perpendicular (x,y) circularly polarized attosecond UV laser pulses with (a, c, e) *co-rotating* and (b, d, f) *counter-rotating* components at wavelengths of (a, b) $\lambda_1 = 3\lambda_2$ ($\omega_2 = 3\omega_1$), i.e., $\lambda_1 = 90$ nm ($\omega_1 = 0.506$ a.u.) and $\lambda_2 = 30$ nm ($\omega_2 = 1.52$ a.u.); (c, d) $2\lambda_1 = 3\lambda_2$ ($2\omega_2 = 3\omega_1$), i.e., $\lambda_1 = 90$ nm ($\omega_1 = 0.506$ a.u.) and $\lambda_2 = 60$ nm ($\omega_2 = 0.76$ a.u.); and (e, f) $3\lambda_1 = 5\lambda_2$ ($3\omega_2 = 5\omega_1$), i.e., $\lambda_1 = 150$ nm ($\omega_1 = 0.304$ a.u.) and $\lambda_2 = 90$ nm ($\omega_2 = 0.506$ a.u.). Pulse intensity $I_0 = 5 \times 10^{14}$ W/cm^2 ($E_0 = 0.12$ a.u.), FWHM = 596 as, CEPs $\phi_1 = \phi_2 = 0$ ($\phi = 0$), and time delay $\Delta\tau = 4.5\tau$ (446 as).

Comparison of MPMDs for different attosecond photoionization schemes in Figs. 2–4 shows that the bursts of the spiral interference patterns are dependent on the helicities of the two circularly polarized UV pulses, i.e., co-rotating or counter-rotating components, and the pulse frequencies ω_1 and ω_2. These spiral MPMDs in fact reflect the maxima of the net fields in Eqs. (5)–(7). For bichromatic circularly polarized attosecond UV pulses at frequencies ω_1 and ω_2, the maxima occur at

$$\cos\frac{(\omega_1 - \omega_2)t}{2} = \pm 1, \quad \text{i.e.,} \quad t = \frac{\tau_0}{m_1 - m_2}, \tag{37}$$

for the co-rotating case and

$$\cos\frac{(\omega_1 + \omega_2)t}{2} = \pm 1, \quad \text{i.e.,} \quad t = \frac{\tau_0}{m_1 + m_2}, \tag{38}$$

for the counter-rotating scheme, with $\tau_0 = 2m_1m_2\pi/E_e$, where $E_e = p^2/2 + I_p = m_1\omega_1 = m_2\omega_2$ $(m_1 > m_2)$ is the photoelectron energy. Therefore, the corresponding numbers of spiral bursts of MPMDs are $m_1 - m_2$ for the co-rotating photoionization and $m_1 + m_2$ for the counter-rotating case.

D. Influence of molecular geometry on MPMDs

We finally show the influence of molecular geometry on the interference patterns by bichromatic circularly polarized attosecond UV pulses. In Figs. 2–4 the ionization processes are presented for the z-aligned molecular ion $H_2{}^+$, i.e., the molecular internuclear R axis is always perpendicular to the polarization (x,y) plane and parallel to the pulse propagation direction. As a result, the molecular photoionization is isotropic in the (x,y) plane, and the molecular geometry can be ignored in the attosecond perturbation ionization models in Eqs. (19)–(36). However, in general for nonspherical molecular Coulomb potentials, multiple nuclear centers result in asymmetric photoionization and distort interference patterns in MPMDs.

In Fig. 5 we display MPMDs for x-aligned $H_2{}^+$, i.e., perpendicular to the propagation direction and in the plane of the laser polarization, by bichromatic circularly polarized attosecond UV laser pulses with co-rotating (left column) and counter-rotating components (right column). The pulse frequencies are $\omega_2 = 2\omega_1$ ($\lambda_1 = 60$ nm and $\lambda_2 = 30$ nm) in Figs. 5(a) and 5(b), $\omega_2 = 3\omega_1$ ($\lambda_1 = 90$ nm and $\lambda_2 = 30$ nm) in Figs. 5(c) and 5(d), $2\omega_2 = 3\omega_1$ ($\lambda_1 = 90$ nm and $\lambda_2 = 60$ nm) in Figs. 5(e) and 5(f), and $3\omega_2 = 5\omega_1$ ($\lambda_1 = 150$ nm and $\lambda_2 = 90$ nm) in Figs. 5(g) and 5(h). The pulse intensities, durations, and CEPs are fixed at $I_0 = 5 \times 10^{14}$ W/cm^2 ($E_0 = 0.12$ a.u.), 12τ (FWHM = 596 as), and $\phi_1 = \phi_2 = 0$. Compared to the results of MPMDs for z-aligned molecules in Figs. 2–4 one sees that no spiral interference pattern can be produced in MPMDs in Fig. 5. For both the co-rotating and the counter-rotating cases MPMDs exhibit a similar distribution structure where photoionization distributions are mainly localized along the y axis, perpendicular to the molecular R axis. The absence of the spiral patterns in MPMDs in Fig. 5 arises from the two-center interference effects in molecular ionization processes, as we show next.

Considering an impulsive, i.e., delta-function field [45], the wave function of the momentum space right after the pulse is given by a Fourier transform of the molecular wave function $\psi_0(t = 0^+)$ [46],

$$\psi(\mathbf{p},0^+) = \exp(-i\mathbf{F}\cdot\mathbf{r})\psi_0(\mathbf{r},t = 0^+), \tag{39}$$

where $\mathbf{p}$ denotes the momentum vector of the photoelectron and $\mathbf{F}$ is the laser-field maximum amplitude. $\psi_0(\mathbf{r},t = 0^+)$ is the initial electronic state wave function. The initial electronic state of $H_2{}^+$ at internuclear distance $\mathbf{R}$ before the interaction is $\psi_{1s\sigma_g} = [\psi_{1s}(-\mathbf{R}/2) + \psi_{1s}(\mathbf{R}/2)]/\sqrt{2}$, i.e., linear combinations of the hydrogenic $1s$ orbital located at $\pm R/2$. The transition amplitude to the continuum state is given by [45]

$$\sigma = \sqrt{2}\cos[(\mathbf{F}+\mathbf{p})\cdot\mathbf{R}/2]\psi_{1s}(|\mathbf{F}+\mathbf{p}|). \tag{40}$$

Equation (40) shows that the effect of the delta pulse is to shift the total distribution by the total amplitude of the field vector $\mathbf{F}$. Since the pulse intensity at high frequencies produces negligible ponderomotive energies $U_p = E_0^2/4\omega^2 \ll I_p$ and $F \ll p$, the pulse-field amplitude $\mathbf{F}$ in Eq. (40) can be ignored to describe the photoionization processes. Then the coefficient $\alpha(\mathbf{p})$ in Eqs. (19)–(34) can be rewritten as

$$\alpha(\mathbf{p}) \sim 2\cos^2(\mathbf{p}\cdot\mathbf{R}/2) = 2\cos^2(pR\cos\theta/2), \tag{41}$$

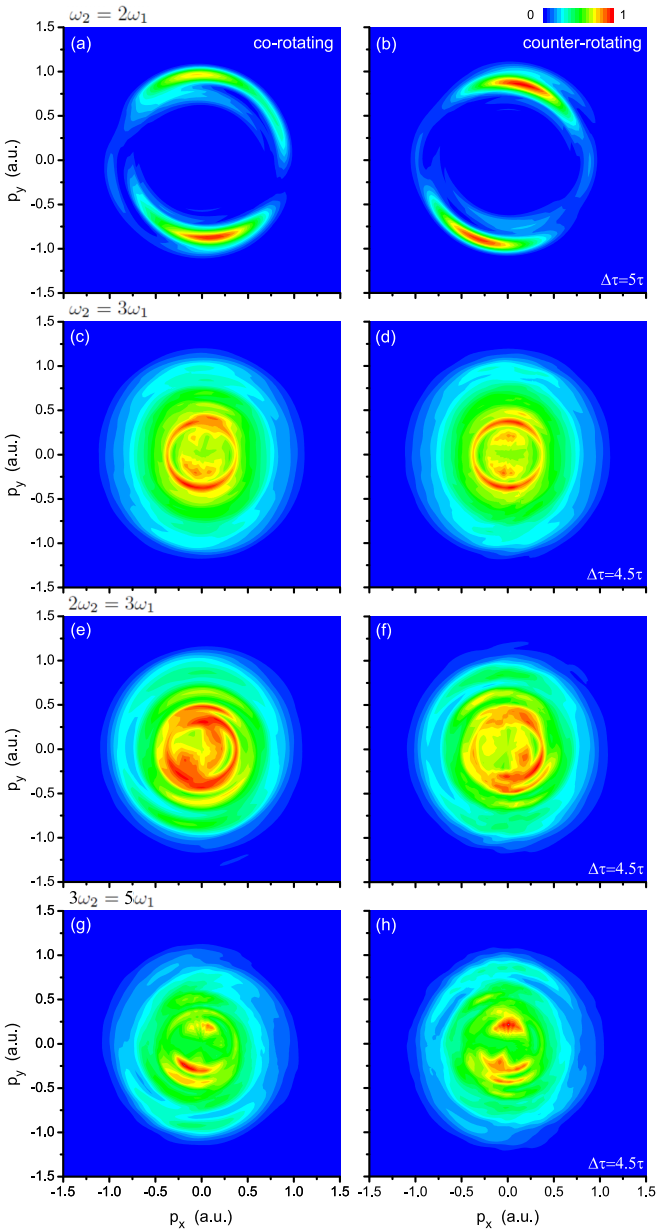

FIG. 5. MPMDs of x-aligned $H_2{}^+$, perpendicular to the laser z-propagation direction, in bichromatic perpendicular (x,y) circularly polarized attosecond UV laser pulses with (a, c, e, g; left column) *co-rotating* and (b, d, f, h; right column) *counter-rotating* components at wavelengths of (a, b) $\lambda_1 = 60$ nm ($\omega_1 = 0.76$ a.u.) and $\lambda_2 = 30$ nm ($\omega_2 = 1.52$ a.u.); (c, d) $\lambda_1 = 90$ nm ($\omega_1 = 0.506$ a.u.) and $\lambda_2 = 30$ nm ($\omega_2 = 1.52$ a.u.); (e, f) $\lambda_1 = 90$ nm ($\omega_1 = 0.506$ a.u.) and $\lambda_2 = 60$ nm ($\omega_2 = 0.76$ a.u.); and (g, h) $\lambda_1 = 150$ nm ($\omega_1 = 0.304$ a.u.) and $\lambda_2 = 90$ nm ($\omega_2 = 0.506$ a.u.). Pulse intensity $I_0 = 5 \times 10^{14}$ W/cm^2 ($E_0 = 0.12$ a.u.), FWHM = 596 as, CEPs $\phi_1 = \phi_2 = 0$ ($\phi = 0$), and time delays $\Delta\tau = 5\tau$ (496 as) or $\Delta\tau = 4.5\tau$ (446 as) are always fixed.

which is a function of the molecular internuclear distance R. Equation (41) represents the ionization of two outgoing electron wave packets emanating from the two nuclear centers. One sees that the distribution $\alpha(p,\theta,R)$ in Eq. (41) is a function of the photoelectron momentum p, the ejection angle θ, and the molecular internuclear distance R. At momentum $p = 0.92$ a.u. and internuclear distance $R_e = 2$ a.u., the corresponding electron wavelength $\lambda_e = 6.85$ a.u. $> R_e$, thus no diffraction occurs [45]. The photoionization distributions mainly lie along the y-perpendicular direction ($\theta = \pm 90^\circ$). The two-center interference in Eq. (41) dominates and suppresses the interference of CEWPs between ω_1 and ω_2 ionization processes. Therefore, the spiral interference patterns in MPMDs for multiple-center ionization models are suppressed, as illustrated in Fig. 5.

IV. CONCLUSIONS

Molecular photoionization of aligned H_2^+ at equilibrium by bichromatic (ω_1,ω_2) circularly polarized attosecond UV laser pulses has been studied from numerical solutions of 3D TDSEs. The molecular internuclear R axis is always aligned along the z or x axes, i.e., parallel or perpendicular, respectively, to the laser propagation direction. Two schemes of photoionization with co-rotating and counter-rotating components, i.e., same and opposite helicities of bichromatic circularly polarized UV pulses in the polarization (x,y) plane are taken into account. With such high-frequency attosecond UV laser pulses, the electron is directly released to the continuum without initiating any additional dynamics with H_2^+ during ionization processes. Photoelectrons with same kinetic energies can be produced in the continuum after absorption of $m_1\omega_1 = m_2\omega_2$ photons, thus triggering multiple-pathway ionization interference effects of CEWPs.

Results show that MPMDs exhibit a signature of spiral interference patterns by bichromatic circularly polarized attosecond UV laser pulses. It is found that the spiral structure strongly depends on the pulse helicities and frequencies ω_1 and ω_2. Altering the pulse CEPs ϕ_1 and ϕ_2 and time delays $\Delta\tau$ can vary MPMDs. We adopt attosecond perturbation ionization models to describe the dependence of the spiral MPMDs on the laser parameters:

(i) *Light helicity*. Spiral interference patterns can be obtained in both *co-rotating* and *counter-rotating* photoionization processes. We present MPMDs for the z-aligned molecular ionization processes with the molecular R axis perpendicular to the laser (x,y) polarization plane. The interference between CEWPs created from two-path ionization by ω_1 and ω_2 pulses results in asymmetric photoionization distributions which are functions of the momentum p and ejection angle θ of the photoelectron and the relative CEP difference ϕ and time delay $\Delta\tau$ of bichromatic pulses, as shown in Eqs. (19)–(34). At the maxima and minima of distributions, the angle θ depends on the momentum p. Altering the relative pulse CEP ϕ leads to an angle shift of the distributions, thus giving rise to a rotation of MPMDs.

(ii) *Pulse frequency*. The spiral bursts in MPMDs are determined by the frequencies of the bichromatic fields. This indicates the essence of the angular momenta and the magnetic quantum numbers in the ionization processes by bichromatic circularly polarized pulses. At energies $p^2/2 + I_p = m_1\omega_1 = m_2\omega_2$ ($m_1 > m_2$) the spiral interference bursts of MPMDs are, respectively, $m_1 - m_2$ for co-rotating cases and $m_1 + m_2$ for counter-rotating schemes.

(iii) *Molecular geometry*. For photoionization of x-aligned H_2^+ with the molecular R axis parallel to the polarization (x,y) plane, the two-center ionization inference results in distributions following the form $\sim \cos(pR\cos\theta/2)$. With these pulses, MPMDs are mainly localized along the perpendicular direction. As a result, the spiral interference patterns in MPMDs are suppressed.

In summary, the spiral interference patterns in MPMDs are shown to be sensitive to the parameters of bichromatic attosecond UV laser pulses and the molecular alignments, thus allowing us to characterize these pulses and monitor the molecular geometry structures in ultrafast photoionization processes with such bichromatic circular attosecond pulses.

ACKNOWLEDGMENTS

The authors thank RQCHP and Compute Canada for access to massively parallel computer clusters and the Natural Sciences and Engineering Research Council of Canada (NSERC), Fonds de recherche du Québec—Nature et Technologies (FRQNT), for financial support through their ultrafast science programs.

[1] A. H. Zewail, J. Phys. Chem. A **104**, 5660 (2000).
[2] A. Stolow and J. G. Underwood, Adv. Chem. Phys. **139**, 497 (2008).
[3] F. Krausz and M. Ivanov, Rev. Mod. Phys. **81**, 163 (2009).
[4] Z. Chang and P. Corkum, J. Opt. Soc. Am. B **27**, B9 (2010).
[5] A. D. Bandrauk, S. Chelkowski, and H. S. Nguyen, Int. J. Quantum Chem. **100**, 834 (2004).
[6] M. F. Kling and M. J. J. Vrakking, Annu. Rev. Phys. Chem. **59**, 463 (2008).
[7] H. C. Shao and A. F. Starace, Phys. Rev. Lett. **105**, 263201 (2010).
[8] V. Despre, A. Marciniak, V. Loriot, M. C. E. Galbraith, A. Rouzee, M. J. J. Vrakking, F. Lepine, and A. I. Kuleff, J. Chem. Phys. Lett. **6**, 426 (2015).
[9] K. Zhao, Q. Zhang, M. Chini, Y. Wu, X. Wang, and Z. Chang, Opt. Lett. **37**, 3891 (2012).
[10] M. Vrakking, Phys. Chem. Chem. Phys. **16**, 2775 (2014).
[11] F. Mauger, C. Chandre, and T. Uzer, Chem. Phys. **366**, 64 (2009).
[12] F. Mauger, C. Chandre, and T. Uzer, Phys. Rev. Lett. **105**, 083002 (2010).
[13] S. Mitryukovskiy, Y. Liu, P. Ding, A. Houard, A. Couairon, and A. Mysyrowicz, Phys. Rev. Lett. **114**, 063003 (2015).

[14] I. Barth, J. Manz, Y. Shigeta, and K. Yagi, J. Am. Chem. Soc. **128**, 7043 (2006).
[15] K.-J. Yuan and A. D. Bandrauk, Phys. Rev. A **91**, 042509 (2015).
[16] F. A. Weihe, S. K. Dutta, G. Korn, D. Du, P. H. Bucksbaum, and P. L. Shkolnikov, Phys. Rev. A **51**, R3433 (1995).
[17] T. Zuo and A. D. Bandrauk, J. Nonlin. Opt. Phys. Mater. **04**, 533 (1995).
[18] A. D. Bandrauk and H. Z. Lu, Phys. Rev. A **68**, 043408 (2003).
[19] P. B. Corkum, Phys. Rev. Lett. **71**, 1994 (1993).
[20] S. Long, W. Becker, and J. K. McIver, Phys. Rev. A **52**, 2262 (1995).
[21] D. B. Milošević and W. Becker, J. Mod. Opt. **52**, 233 (2005).
[22] F. Ceccherini, D. Bauer, and F. Cornolti, Phys. Rev. A **68**, 053402 (2003).
[23] A. Fleischer, O. Kfir, T. Diskin, P. Sidorenko, and O. Cohen, Nat. Photon. **8**, 543 (2014).
[24] L. Medisauskas, J. Wragg, H. van der Hart, and M. Y. Ivanov, Phys. Rev. Lett. **115**, 153001 (2015).
[25] K. J. Yuan and A. D. Bandrauk, J. Phys. B **45**, 074001 (2012); Phys. Rev. Lett. **110**, 023003 (2013).
[26] E. Cunningham and Z. Chang, IEEE J. Select. Topics Quantum Electron. **21**, 8700806 (2015).
[27] C. A. Mancuso, D. D. Hickstein, P. Grychtol, R. Knut, O. Kfir, X.-M. Tong, F. Dollar, D. Zusin, M. Gopalakrishnan, C. Gentry, E. Turgut, J. L. Ellis, M.-C. Chen, A. Fleischer, O. Cohen, H. C. Kapteyn, and M. M. Murnane, Phys. Rev. A **91**, 031402(R) (2015).
[28] K. J. Yuan and A. D. Bandrauk, Phys. Rev. A **92**, 063401 (2015).
[29] J. M. Ngoko Djiokap, S. X. Hu, L. B. Madsen, N. L. Manakov, A. V. Meremianin, and A. F. Starace, Phys. Rev. Lett. **115**, 113004 (2015).
[30] A. D. Bandrauk and K. J. Yuan, in *From Atomic to Mesoscale: The Role of Quantum Coherence in Systems of Various Complexities*, edited by S. A. Malinovskaya and I. Novikova (World Scientific, Singapore, 2015), Chap. 10.
[31] T. Fan, P. Grychtol, R. Knut, C. Hernández-García, D. D. Hickstein, D. Zusin, C. Gentry, F. J. Dollar, C. A. Mancuso, C. W. Hogle, O. Kfir, D. Legut, K. Carva, J. L. Ellis, K. M. Dorney, C. Chen, O. G. Shpyrko, E. E. Fullerton, O. Cohen, P. M. Oppeneer, D. B. Miloševic, A. Becker, A. A. Jaron-Becker, T. Popmintchev, M. M. Murnane, and H. C. Kapteyn, Proc. Natl. Acad. Sci. USA **112**, 14206 (2015).
[32] K.-J. Yuan and A. D. Bandrauk, Phys. Rev. A **84**, 023410 (2011); K.-J. Yuan, H. Lu, and A. D. Bandrauk, *ibid.* **92**, 023415 (2015).
[33] A. D. Bandrauk and H. Shen, J. Chem. Phys. **99**, 1185 (1993); A. D. Bandrauk and H. Lu, J. Theor. Comput. Chem. **12**, 1340001 (2013).
[34] K. J. Yuan, H. Z. Lu, and A. D. Bandrauk, Phys. Rev. A **83**, 043418 (2011).
[35] C. A. Leach and R. E. Moss, Annu. Rev. Phys. Chem. **46**, 55 (1995).
[36] M. Garg, A. K. Tiwari, and D. Mathur, J. Phys. Chem. A **116**, 8762 (2012).
[37] K. F. Lee, D. M. Villeneuve, P. B. Corkum, A. Stolow, and J. G. Underwood, Phys. Rev. Lett. **97**, 173001 (2006).
[38] K. J. Yuan and A. D. Bandrauk, Phys. Rev. A **85**, 013413 (2012).
[39] E. A. Pronin, A. F. Starace, M. V. Frolov, and N. L. Manakov, Phys. Rev. A **80**, 063403 (2009).
[40] E. A. Pronin, A. F. Starace, and L. Y. Peng, Phys. Rev. A **84**, 013417 (2011).
[41] J. Bakos, A. Kiss, L. Szabó, and M. Tendler, Phys. Lett. A **41**, 163 (1972).
[42] H. L. Kim and R. Bersohn, J. Chem. Phys. **107**, 4546 (1997).
[43] Z. M. Wang and D. S. Elliott, Phys. Rev. Lett. **87**, 173001 (2001).
[44] K. J. Yuan, S. Chelkowski, and A. D. Bandrauk, Chem. Phys. Lett. **592**, 334 (2014); J. Chem. Phys. **142**, 144304 (2015).
[45] T. Zuo, A. D. Bandrauk, and P. B. Corkum, Chem. Phys. Lett. **259**, 313 (1996).
[46] K. J. Yuan and A. D. Bandrauk, Struct. Dynam. **2**, 014101 (2015).